

IMPROVEMENT AND CONTROL TRAJECTORY TRACKING OF A THREE-AXIS MANIPULATOR FOR NEW TRAINING STRATEGIES

Patryk MIETLIŃSKI*, Michał JAKUBOWICZ*, Lidia MARCINIAK-PODSADNA*, Michał WIECZOROWSKI*

*Faculty of Mechanical Engineering, Division of Metrology and Measurement Systems, Poznan University of Technology, M. Skłodowskiej-Curie 5, 60-965 Poznań

patryk.mietlinski@put.poznan.pl, michal.jakubowicz@put.poznan.pl, lidia.marciniak-podsadna@put.poznan.pl, michal.wieczorowski@put.poznan.pl

received 04 April 2024, revised 21 May 2025, accepted 16 June 2025

Abstract: This study discusses the development of training strategies for RRR (3 revolute joints) triaxial manipulators. Two robot structures and a control phantom were constructed using incremental technology. An universal algorithm was developed to process and autonomously repeat the trajectories of robot movements by imitation and learning. The coordinates of the model articulated positions were then saved as coordinates of the manipulator position. For validation purposes, the newly developed training strategies and the repeatability of robot movements were tested in stages. After the first stage of testing in terms of positioning accuracy, structural changes were introduced in the robot by mechanical engineering to improve its manipulation quality. Next, another training strategy for the improved robot version was developed for the same movement algorithm. This demonstrates the applicability of the developed control system in applications with different structures and requirement for high control-command quality (possibility of using the developed algorithm in various robot designs). Experimental results showed that the function of the developed RRR manipulator algorithm enabling the imitation of phantom trajectories and their learning and memorization, along with the consideration of individual training strategies, can be applied to differing structures, achieving positioning accuracy comparable to that of high-class motion equipment, and facilitating navigation of individual robot members. The system composed of the simplified physical model and the manipulator can directly simplify and globalize the control of the robot over significant distances. Additionally, the positioning accuracy was tested using the photogrammetric method, which is a complete novelty in robot positioning research. Furthermore, it was demonstrated that for the first construction of the robot, it is possible to achieve an accuracy of ±1 mm in the automatic replay mode. Moreover, a construction accuracy of ±0.52 mm at a maximum speed of 0.025 s/1° can also be accomplished after manual repeat of the different model movements, i.e., after a learning procedure.

Key words: three-axis manipulator, RRR robot, training strategies, 3D scanners, robot programming, positioning accuracy

1. INTRODUCTION

In recent years, there has been a continuous and dynamic development of industry, resulting in the Fourth Industrial Revolution or Industry 4.0. The revolution aims to automate production and increase the mobility of individual elements of the product chain [1, 2]. Gradually, companies are introducing autonomous solutions to their factories that enable virtually maintenance-free work on production stands [3, 4]. The human factor is definitely being replaced by manipulators and both automatic production [5] and transport devices [6], leaving only supervisory and control roles [7] for humans. However, such autonomous solutions are required to be universal and have high implementation precision, as described by Jermak Cz. J. et al [8], and Jakubowicz M. et al. [9]. Such solutions require substantial financial outlays, the profitability of which is achieved only after a prescribed, usually long, period of time.

Existing methods for manipulating components and subassemblies involved in the overall production process are of key importance for assembly and internal aspects of interstate handling [10, 11]. Some of the first studies that raised issues regarding the need to automate manipulation operations in order to improve industrial operations related to the control and quality of unattended

manufacturing of elements; they were published in 1973 by Häuschen H. [12] and Warnecke H. J. et al. [13]. Moreover, many contemporary authors have emphasized the importance of automating manipulation processes and problems related to their implementation [14, 15]. Furthermore, additional considerations related to the results of control accuracy that enable the determination of the potential quality of positioning.

Quality requirements are constantly growing and production technologies keep developing; hence, more accurate and universal measurement systems and methods [16, 17, 18] as well as diagnostics have to be applied [19]. Articulated robots that enable numerical control along several axes are currently the most frequently used manipulating machines, enabling dimensional and geometric control. The universality of 3D scanner solutions was evidenced by Andrzejewski J. [20]. In most cases, their programming is based on the online programming procedure described by Chen X. et al. [21] and Maini P. et al. [22]. Offline programming is also possible, as reported by Mitsi S. et al. [23] and Larkin N. et al. [24]. In all the above cases, the developer stays far from the operation site. This creates the problem of lack of intuitive programming.

There are also reports of hybrid methods using offline and online programming [25, 26]. However, such solutions have limited applicability and are dedicated to specific purposes. In this respect,

DOI 10.2478/ama-2025-0045

it may be helpful to develop a robot operation mode by tracking the trajectory of motion of a simplified physical model used for innovative programming of manipulators in accordance with the guiding principle of Industry 4.0 [27].

In industrial applications related to working machines, manipulators, and their drives, the main criterion to determine their suitability for a particular use is to obtain the best possible positioning accuracy [28]. The operation algorithm is based on obtaining the closest position to the original set position in each pass and cycle of device operation. The main objective for the control system, mechanical structure, and developed program, which are collaboratively responsible for realizing the manipulator movement, is to obtain maximum precision while maintaining the basic motion conditions of the manipulator displacement trajectory. Hybrid methods allowing offline and master-slave robot programming are commonly used [29-31]. Research on such solutions has also been carried out [32-34]. However, a constant limitation is the inability to apply one universal algorithm to various mechanical manipulator designs. It is necessary to create separate control programs for separate mechanical solutions of robots. None of the authors have previously attempted to apply the same control algorithm to two completely different robots.

It is important to note that autonomous solutions are gradually being introduced, enabling nearly maintenance-free operation of production workstations. The human factor is being replaced by manipulators and automatic production and transport devices, leaving only supervisory and control functions to humans. These solutions must be universal and characterized by high implementation precision, which involves significant financial investments that typically pay off only after a longer period of time.

In the context of Industry 4.0, the application of artificial intelligence (AI) techniques plays a key role in optimizing production processes. Azizi et al. [35] presented a hybrid AI algorithm for optimizing RFID network planning, which is significant for efficient resource management in modern production systems. In another study, Azizi [36] proposed the use of artificial neural networks to optimize the dynamic behavior of robotic arms, contributing to increased sustainability in Industry 4.0. Moreover, Latifi-Navid et al. [37] developed an autonomous robot for collecting tennis balls, using LiDAR for environmental mapping and a camera for ball detection, demonstrating the practical application of AI in mobile robotics. In the field of mechanical systems control, the use of a Ring Probabilistic Logic Neural Network (RPLNN) to design an active vehicle suspension controller was presented by Azizi et al. [38], showcasing AI's potential in improving the mechanical stability of structures.

All these studies emphasize the importance of integrating Al techniques into various aspects of industrial automation, from network planning to the control of robots and mechanical systems. However, despite the advances in this field, there remains a need for further research into universal control algorithms that could be applied to different manipulator designs. In response to this need, the present study focuses on the development and implementation of a universal control program that is not dedicated to a single type of manipulator but can be directly applied to various structures.

Therefore, the authors decided to create a universal control program that would not be dedicated only to one type of manipulator but could be directly applied to separate structures. For this purpose, it was decided to design and build two different manipulators from scratch. Then it was decided to apply the same control algorithm to them, based on master-slave programming using a control phantom (the ability of the manipulator to repeat the phantom's movements and then recreate them as faithfully as possible). Next,

it was decided to perform an appropriate learning procedure using a control phantom for each structure and then recreate the same trajectories for each robot. Then, in order to verify the quality of positioning, it was decided to perform positioning quality tests using the photogrammetric method. None of the authors attempted to investigate positioning accuracy using structured light scanners. According to the authors of the article, considering the measurement accuracy of such a measurement system, it is a reliable source of obtaining measurement information for the required positioning quality measurements. This metrological approach is another novelty when testing the accuracy of manipulator positions. Previous studies focused on the optimization of manipulators to obtain better metrological properties [39, 40]. However, the complex design and implementation of a universal, intuitive control algorithm using a robotic phantom that enables its application in various types of automatic manipulation structures, allowing for the development of specific training strategies for specific tasks, have not been described in the literature yet. Therefore, in this study, a research stand was prepared in a configuration that enables the analysis of training strategies using the developed phantom-manipulator control algorithm on various types of structures. In addition, the accuracy of the manipulability for specific robots was evaluated. Thus, a novel analysis is proposed that provides data for a clear comparison of the positioning quality performance of two articulated manipulators with significant design differences.

Previous scientific publications have not undertaken a comprehensive analysis of the issues related to the evaluation of positioning accuracy in three-axis manipulators in the context of the developed control algorithms. There has also been a lack of comparative approaches that would include real-world verification of trajectory reproduction quality in reference to programmed motion paths.

In response to this research gap, the authors of this study are the first to propose a method for verifying and assessing the positioning accuracy of manipulators using advanced, previously unused measurement technologies in this area—namely, a structured light scanner and a multisensor coordinate measuring machine (CMM).

The application of these advanced metrological tools enables precise reproduction and evaluation of deviations from the predefined trajectory, allowing for an objective assessment of the effectiveness of the designed control algorithms. Similar approaches to the assessment of manipulator positioning accuracy have previously been explored by Wang et al. [41], who utilized 3D scanning techniques to evaluate the precision of industrial robots, and by Chen et al. [42], who employed multisensor measurement systems for analyzing positioning accuracy in robotics.

Furthermore, research conducted by Li et al. [43] demonstrated that integrating structured light scanning with robot control significantly enhances the quality of trajectory reproduction. However, these authors did not validate or compare their methods using different metrological systems, nor did they attempt to adapt their solutions to various types of manipulators.

Therefore, the present study aimed to address this gap by comparing two distinct measurement systems in the context of positioning accuracy testing and evaluating the adaptability of the developed control algorithm to different robotic structures.

The proposed approach represents an innovative contribution to the development of methods for evaluating the performance of industrial manipulators, particularly in terms of their adaptability to diverse applications within the Industry 4.0 environment, where precision and flexibility of control are of paramount importance.



2. CONSTRUCTION AND CONTROL ALGORITHM

2.1. Concept of manipulator constructions

Two different manipulators were used to compare the usefulness and universality of the devel-oped control system based on serial motion kinematics. In this concept, the link with the attached force performing the kinematic transfer is a unit of motion of the kinematic set. A kinematic diagram must be defined to specify the basic position of the members, their interconnections and positions, and dimen-sional and geometric descriptions. Therefore, the manipulator structure is designed to integrate robot elements and realize the relationship between sub-assemblies for the selected system. A kinematic diagram of the compiled RRR robot is shown in Fig. 1. Each member moves along a particular axis and is connected to the rest of the system in an articulated manner. The integrated movement of each axle enables the manipulator to be controlled in the working space and realization of the assigned tasks.

To implement the actual design of the manipulator, a non-additive manufacturing method was employed. This gave rise to the expected behavior of the components required for their realization while maintaining a relatively short manufacturing time (printing speed of approximately 50 mm/s). A biodegradable polylactide called PLA was used as the manufacturing material. This material is charac-terized by a small processing cramp resulting from the ease of FDM printing.

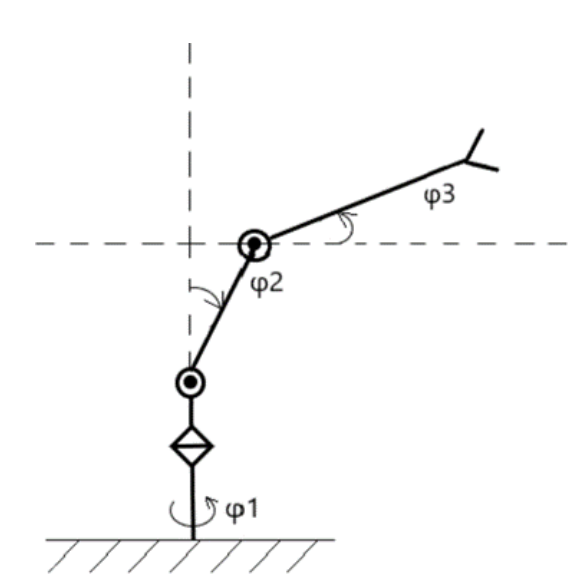


Fig. 1. Kinematic diagram of the RRR serial robot

In addition, pilot kinematic simulations of planned structures were performed for pilot purposes, assuming conditions associated with the type of manipulation of RRR robots. These simulations enabled the analysis of the Denavita–Hartenberg methodology used by Qingbing Ch. et al. [44] and Li H. el. al. [32]. In the case of the manipulator, RRR holds all the rotating connectors. For such a combination, the angle of rotation θ^i is always variable, the linear displacement d_i is always constant, and each connector has only one degree of freedom. Therefore, to determine the location of the individual components of the manipulator in space, the local coordinate systems at each joint must be defined:

$$ROT\left(X,\theta^{i}\right)\begin{bmatrix} cos\theta^{i} & -sin\theta^{i}cos\alpha^{i} & sin\theta^{i}sin\alpha^{i} & a_{i}cos\theta^{i}\\ sin\theta^{i} & cos\theta^{i}cos\alpha^{i} & -cos\theta^{i}sin\alpha^{i} & a_{i}sin\theta^{i}\\ 0 & sin\alpha^{i} & cos\alpha^{i} & d_{i}\\ 0 & 0 & 0 & 1 \end{bmatrix} (1$$

The simulations aimed to obtain information on the marginal positions and trajectories of robot movements to develop an initial strategy for the control algorithm. The resulting information enabled us to focus on specific problematic aspects of robot control. Therefore, by recasting the parameters related to the movement of the joints themselves and the homogeneous transformation matrix (Equation 1), a matrix defining the individual marginal positions of the joints and end-end elements of the manipulator (Fig. 2) was obtained. Analyses, calculations, and simulations were performed using the RoboAnalyzer v. 7.5 software (Mechatronics Lab, India).

Fig. 2. Form of the homogeneous transformation matrix; from the left to the right: form of the third joint relative to the robot arm end; form of the arm end relative to the base coordinate system (source: RoboAnalyzer)

Based on these matrices, the trajectory of robot movements could be simulated. These included the coordinates of the initial points from which the movement of the robot arm was started, and the marginal coordinates of the reference point for the extreme position. Thus, it was possible to delineate and visualize both the working space and nature of the kinema-magnetic manipulation system (Fig. 3).

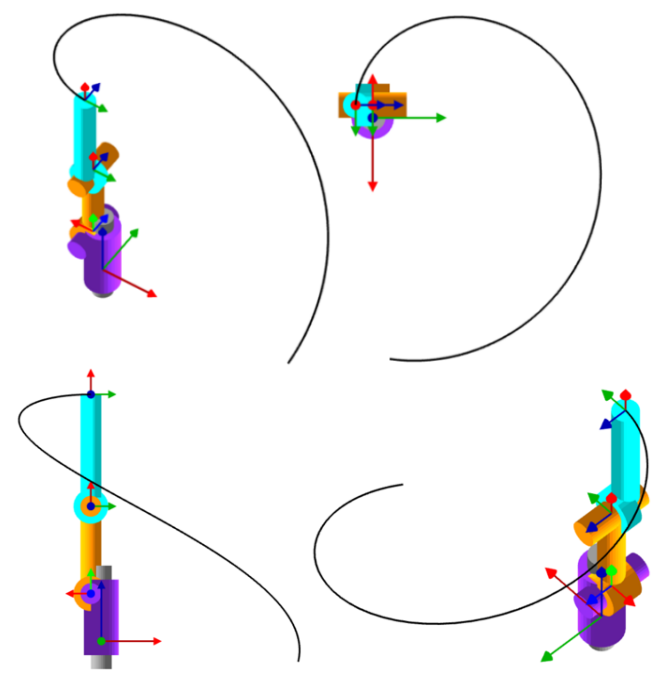


Fig. 3. View of the drawn manipulator trajectory for the maximum extreme position of the robot arm (source: RoboAnalyzer)

DOI 10.2478/ama-2025-0045

2.2. Construction of the first manipulator

The design concept is based on a structure consisting of four modules (Fig. 4). The first segment is the base and fixation of the entire robot on the ground. This is an element of a structure that cannot be moved when the manipulator is in operation. Moreover, it acts as a support for the first motor that rotates in the first direction. The next module considers movement along the x-axis. It was attached directly to the shaft of the first drive and located directly above the base module, allowing eccentric movement with respect to the shape of the bases. Another module was attached in a direction perpendicular to the segment, allowing movement along the xaxis. This enables the next movement along the y-axis. This is realized by means of a motor fixed to the previous component at an angle of 90° in the relation shaft - i.e., the base. The last arm, which is an extension of the previous subassembly moving along the z-axis, was subsequently installed. The beginning of this module was mounted on the shaft of the third motor, which was attached to the end of the previous segment. These arms were connected parallel to the base and previous module. At the end of the last segment, it was possible to rigidly fix the robot tool with possibility of articulation. In the described structure, individual shafts of servos responsible for specific movements are connected directly to movable modules without additional connecting elements. Thus, it was possible to eliminate the additional play on the movable joints. Locating the motors in series with each member successively increased the forces and moments as the number of segments increased with respect to the distance from the attachment point. As a result, the engine that was farthest from the point where the tool was connected to the manipulator was loaded the most. Such a structure reduced the stiffness of the machine, thereby reducing the positioning accuracy. However, it enabled a guick and dynamic response to changes during control.



Fig. 4. Model view of the first manipulator (left side) and view of the finished construction of the first manipulator (right side)

2.3. Construction of the second manipulator

After the first construction was completed, some changes were introduced. These changes ad-dressed two aspects. First, the influence of mechanical modifications of individual robot members on the quality of positioning was considered. Second, the feasibility of applying the same algorithm to two different RRR robot constructions was verified. Thus, the usefulness of the executed program and the possibility of introducing and correcting the operation for different manipulators could be evaluated.

The design of the second robot was based on a modular structure with serial kinematics (Fig. 5). A fixed base was made to

support the entire robot. Then, through the use of a bolt and nut, bearings, and small spherical balls, the first movable module realizing the movement along the x-axis was mounted. An important aspect was the additional use of a reduction gear on the servo and the component carry-ing out the movement along the x-axis. This allowed for the reduction of the forces and moments on the shaftfirst engine. On the first movable module, there were two servos that moved along the y- and z-axes. In this way, additional moments arising on individual parts of the arm due to the mass of the motors themselves were reduced. Because all servos were mounted at a considerable distance from the end of the arm, transmitting the drive to the individual joints became a problem. Therefore, the arm was moved along the y- and z-axes by connecting the individual elements of the movement mecha-nisms by attaching rigid tendons to them. Thus, it was possible to coordinate the movement of the arm along both the y- and z-axes. Owing to the use of this type of drive ratio, it was possible to reduce the weight of the arm and control the stiffness of the manipulator's movement at the expense of the dy-namics of its reaction. Unfortunately, such a solution introduced the possibility of creating additional play in the entire system and the necessity to control the condition of the connection

in the movement areas of the main joints and connection points of the tendons with individual movable elements of the arm.



Fig. 5. Model view of the second manipulator (left side) and view of the finished construction of the second manipulator (right side)

2.4. Control algorithm

We decided to combine several types of control, creating an original method for designing the tra-jectory of the manipulator's movements. Through the activation of potentiometers in the form of a simplified physical model and the separation of the electronic system of the robot and phantom, the manipulator became a completely independent device. This enabled online robot programming exactly where it was supposed to work - a phantom connected directly to the manipulator - and offline pro-gramming such that on the basis of the model's movements, positions could be saved in the electronic system. Then, by connecting the system to the robot, the saved program was recreated. These two methods for planning movements are related to teach-in programming, except that the trainer need not be in front of the machine. In addition, with the appropriate use of specific data transfer, it is possi-ble to train the robot in teleconference mode. Therefore, the developed solutions enabled the combi-nation of all types of control: direct, indirect, and the use of direct programming languages. Additional-ly, PTP (pointto-point) control was used. This allowed the manipulator to move smoothly from point to point (stored in memory) according to the set motion trajectories by moving the phantom. In addition, by sciendo

writing program code, the trajectories of the robot's movement could be manually entered and set. In addition, it is possible to determine the "home" position of the manipulator, from which it always starts the execution of the stored program, and the speed of the motor movement, thereby adjusting the positioning accuracy. The logic diagram of the algorithm is shown in Figure 6.

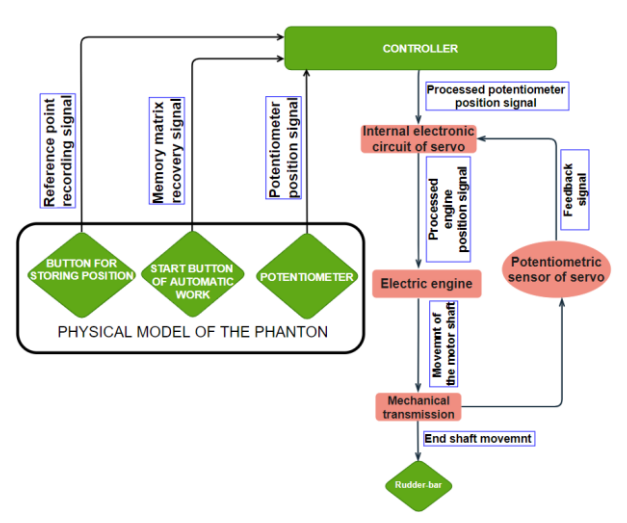


Fig. 6. Control algorithm diagram

The value given at the input in the transmitter is read by the receiver and compared with the output signal changed by the converter. This is how errors arise. They are fed to the corrective element and amplifier. The amplified signal goes to the actuator, that is, the DC electric motor. Its rotation value is the output value of the entire system. The servomechanism is a follow-up system that eliminates the displacement error. It does not control the entire object but only its drive, i.e., the engine. Consequently, the execution track is improved. The integral nature of the servo practically ensures zero static error while maintaining a high gain in the main path, improving the system's ability to follow changes in the input signal. Depending on the difference between the current and defined positions, the motor is driven by a signal with a greater or lesser duty cycle. The running motor, which drives the mechanical transmission, also rotates the potentiometer, which is permanently connected to the transmission. The movement of the potentiometer causes a change in resistance, which is read by the internal system; if it reaches an appropriate defined value for a given input signal, the motor stops working because the servo has reached the prescribed position.

3. RESEARCH METHODOLOGY

3.1. Research methodology of first construction

Stage I

The key movements of the manipulator implementing the trajectories are the reconstruction of straight lines and one angle. Therefore, we decided to execute a pattern printed on paper (Fig. 7). The geometry of five pairs of parallel lines was prepared with distances of 10, 15, 20, 25, and 30 mm and a right angle.



Fig. 7. Reference geometric view

In the first phase, the robot imitated the movements of the phantom at a distance of 500 mm from the manipulator. Additionally, when imitating the movements, the robot marked the developed geometry (one of the six drawn) on a reference sheet attached to its arm with a marker. During the movements, the learning process took place, and the reference points were recorded in the memory of the manipulator. After the learning process, the drawn geometry was repeated 30 times with independent (automatic mode) execution of the developed training strategies to recreate the memorized trajectories. The speed of the movement of the manipulator reached 0,025 s/1°. A blank white sheet of paper was placed at the base of the robot before each cycle was performed in playback mode. During the implementation of the learned trajectories, the manipulator marked the remembered key movement for a given strategy in accordance with the pattern for a given geometric case. After each cycle, the page was changed.

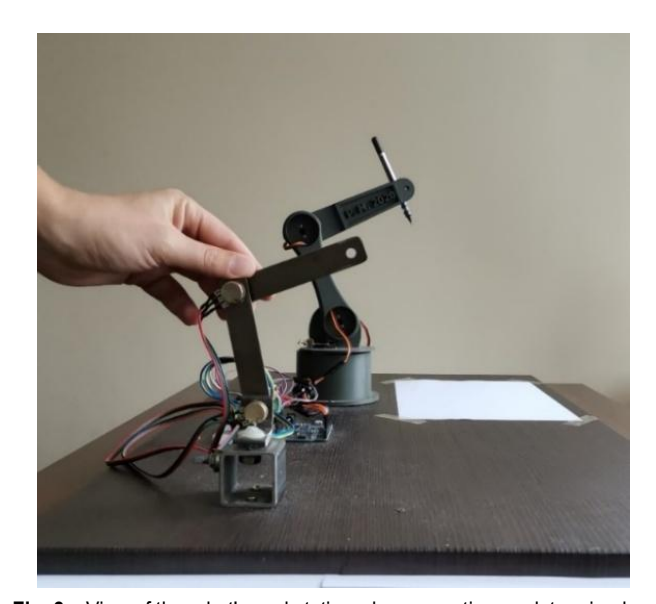


Fig. 8. View of the robot's workstation when executing predetermined geometries

Stage I

After the completion of Stage I, the quality of the developed training strategies had to be verified. Therefore, positioning accuracy was checked by examining the quality of the marked geometries. The dimensions of the printed standard were measured. Additionally, all the geometries marked on the sheet by the manipulator were realized in accordance with the printed standard. Hence, it was necessary to verify the created shapes using the actual dimensions obtained after printing.

For the above analysis, a test was carried out on the Baty Venture XT multisensory measuring device (Fig. 9) equipped with a self-calibrating zoom lens with a magnification of up to 12× and an auto-focus system. This device enables measurements with a resolution of 0.5 μm . The measurement structure was based on optimization using the finite element method.

sciendo

DOI 10.2478/ama-2025-0045

The test consisted in measuring the distance between two parallel lines or an angle. The center of each line was determined. The points of geometry were then detected and displayed in the measuring system of the machine. Thus, it was possible to create lines from the selected points and measure the distance between them. To ensure the test reliability, each geometry was measured 30 times.

After conducting research on the dimensions, it was necessary to verify the positioning accuracy of the manipulator itself. To this end, we analyzed the dimensions of the geometry created in automatic mode by the robot after performing the learning procedure. Each sample was tested. Thus, a set of 30 measurements was obtained for each geometry. The samples were measured in the same manner as the standard dimensions were checked. The results of the analysis were saved after each measurement.



Fig. 9. Test stand including the Baty Venture XT measuring machine

3.2. Research methodology of second construction

Analysis of the first structure led to consideration of the second structure. In this case, we intro-duced an application aspect to the study. The manipulator was supposed to transfer the designed element from one place to another. Three separate sequences were analyzed. In each of them, the ma-nipulator took the object from the same place and then transferred it to a given distance.

Each se-quence was preceded by a trajectory-learning procedure in which the transfer distance was directly defined. The manipulator performed three sequences. In each of them, the element was moved to a different distance successively: 84.0 mm, 121.2 mm, and 204.2 mm.

An important issue, as in the first construction case, was to start the sequence operation always from the same place – i.e., the home position. This guaranteed the closest similarity of movement and hence, the most reliable mapping of the trajectory and displacement of the transferred element. In each sequence, the manipulator per-formed 30 repetitions (cycles) in accordance with previously learned trajectories (in total, 90 element movements were performed).

A 3D scanner, Atos Core 300, was used to test the accuracy, together with the dedicated Atos software that enables measurement with a resolution of up to 0.182 mm. 3D scanning uses digitization, which is the process of applying data from real objects to digital ones. The measurements provide a spatial cloud of points that can be polygonized into a mesh of triangles.

Based on the scanned data, a CAD model of the real station was developed, and the starting point of movement was fixed. Then, the real object displacement was analyzed in relation to the fixed start and end points of the movement, and it was possible to measure a real object in relation to its nominal values.

A view of the test stand during the examination of the second structure from GOM INSPECT 2018 Professional software (GOM GmbH, Germany) is presented in Fig. 10.

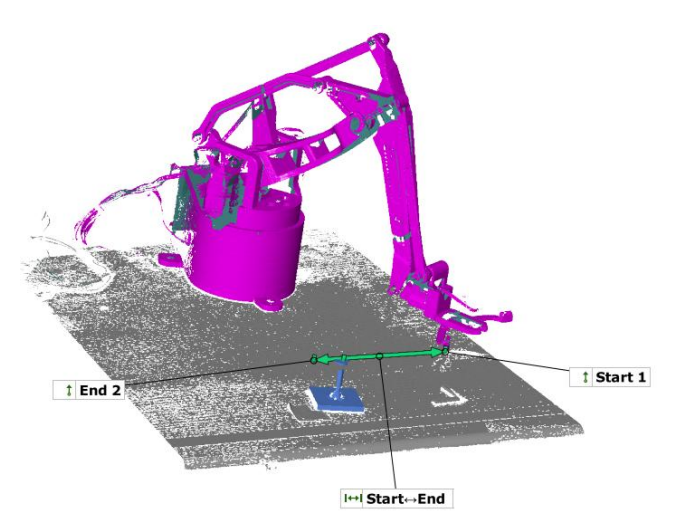


Fig. 10. View of the test stand during the examination of the second structure using GOM software

After each implementation of the trajectory cycle in each sequence, the actual distance of object displacement was measured using a 3D scanner. The original position of the item and position of the item after transfer were measured. Both measurements in the cycle were taken against the previously determined reference points. The relative difference between both positions resulted in a distance displacement in the three axes, and thus, the corresponding total displacement. Consequently, it was possible to determine how the position of the transferred object in relation to its initial position changed in individual cycles for each sequence. The difference between the value of the set distance during the learning procedure and the value obtained in a particular cycle resulted in deviation from the original value. Accuracy analysis was conducted based on the obtained data.

4. RESULTS AND DISCUSSION

4.1. Results of first construction

The results of the measurements of the proposed standard are presented in Table 1. The results are listed for all the considered geometries and calculations on the basis of the obtained values. Table 1 includes drawing distances of 10, 15, 20, 25, and 30 mm, and an angle of 90°. Similar to a previous study [45], for the analysis of results, statistical parameters were used, such as standard deviation σ , skewness A, and kurtosis K.

The standard deviation can be determined from the following expression:

$$\sigma = \sqrt{\frac{1}{(n-1)} \sum_{i=1}^{n} (x_i - \bar{x})^2}$$
 (2)



where \bar{x} is mean value calculated from the following formula:

$$\bar{x} = \frac{1}{n} \sum_{i=1}^{n} x_i \tag{3}$$

where *xi* is a measurement result *n* denotes the number of repetitions.

Properties were determined using a series of 30 repetitions (n = 30).

Skewness A was determined as follows:

$$A = \frac{n}{(n-1)(n-2)} \sum_{i=1}^{n} \left(\frac{x_i - \bar{x}}{\sigma} \right)^3 \tag{4}$$

Kurtosis K was determined from the following expression:

$$K = \left\{ \frac{n(n+1)}{(n-1)(n-2)(n-3)} \sum_{i=1}^{n} \left(\frac{x_i - \bar{x}}{\sigma} \right)^4 \right\} - \frac{3(n-1)^2}{(n-2)(n-3)}$$
 (5)

To evaluate the measurement uncertainty of the determined parameters, the type-A method for estimating the uncertainty was used.

Extended uncertainty U0,95 is obtained by multiplying the standard deviation by the appropriate factor:

$$U_{0,95} = k \cdot \frac{\sigma}{\sqrt{n}} \tag{6}$$

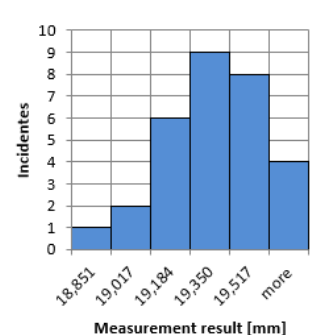
For the calculations, k = 1.960 was applied, which corresponds to the quantile of the Gaussian distribution. If there are less than 30 repetitions, the coverage factor assumes the value of the Student's quantile distribution. For example, for a confidence level P = 95%, the quantile of the Student's distribution is $t\alpha = 2,262$. To check the normality of the random variable, the $\chi 2$ compliance test was used; N indicates the number of repetitions [45, 46].

Results for R were calculated as the difference between maximum and minimum values.

Based on the obtained results and calculations, an analysis was conducted; exemplary results are presented in Fig. 11.

Tab. 1. Results of the reference measurements and their calculations

	10 mm	15 mm	20 mm	25 mm	30 mm	90°
Mean	9.125	14.356	19.284	24.068	28.904	89.876
Max	9.398	14.604	19.683	24.315	29.148	89.938
Min	8.746	14.148	18.851	23.733	28.624	89.803
R	0.652	0.456	0.832	0.582	0.524	0.135
σ	0.178	0.140	0.189	0.177	0.132	0.034
Α	-0.589	0.342	-0.093	-0.114	0.104	0.012
Κ	-0.197	-0.743	-0.042	-1.230	-0.120	-0.412
$U_{0.95}$	0.064	0.050	0.068	0.063	0.047	0.012



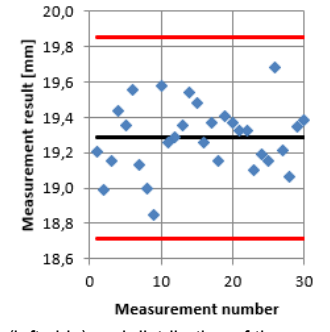


Fig. 11. Value distribution histogram (left side) and distribution of the result values $\pm 3\sigma$ (right side) for parallel lines 20 mm apart

The above histogram (Fig. 11) for parallel lines 20 mm apart takes an asymmetric form close to the normal distribution, with a clear peak reached for the values in the range of 19.350 mm. On this basis, it can be concluded that the mean value (19.284 mm) was recorded on one side of the distribution. This proves that the lower limit of the results and density of the measurements are close to the mean values. Additionally, Fig. 11 shows that most of the measurement points oscillate around the mean value. This was confirmed by the distribution of results. Note that most measurements were at or above the mean value. Additionally, all values were within the range (+ 3σ ; - 3σ). The difference between the maximum and minimum values was 0.832 mm. The skewness coefficient is negative, but remains at a very low level (-0.093), with little scattering. The kurtosis was negative for all measurements, which means scattering around the calculated mean of measurements. However, kurtosis values relatively close to zero indicate that the concentration of results is close to the average distribution. The quality of manipulator positioning was analyzed on the basis of the measurement results of the actual pattern.

For all geometries, calculations were made on the basis of the obtained values presented in Table 2 for the original structure geometries. The same parameters were used for analysis. Moreover, the same graphs were created as in the case of reference.

Tab. 2. Results of geometric measurements made by the robot and their calculations

	10 mm	15 mm	20 mm	25 mm	30 mm	90°
Mean	9.711	14.614	19.004	24.448	29.174	90.100
Max	9.911	14.895	19.280	24.794	29.371	91.253
Min	9.450	14.200	18.680	23.825	28.940	88.048
R	0.461	0.695	0.600	0.969	0.431	3.205
σ	0.130	0.191	0.177	0.274	0.135	0.819
Α	-0.166	-0.171	-0.122	-0.470	-0.381	-0.530
K	-0.884	-0.888	-1.127	-0.790	-1.240	-0.336
$U_{0.95}$	0.047	0.068	0.063	0.098	0.048	0.293

Concerning the analysis of the geometry performed by the manipulator, it can be concluded that the average values of the results for each case are very close to the reference ones. Kurtosis values for all cases, similar to the pattern analysis, were below zero. Its mean value is greater than the values of all reference values; therefore, it can be concluded that the dispersion is also greater. This is justified because it is difficult to obtain a high level of a small range of results using the teaching machine.

Then, the results had to be interpreted and compared in the form of a relative error:

$$\delta = \left| \frac{\overline{x_i - W}}{W} \right| \cdot 100\% \tag{7}$$

where \bar{x} is the mean value

W denotes the reference value.

For the calculations using Equation 7, a graph was plotted (Fig. 12) showing the distribution of the relative error for the selected geometry made by the robot in relation to the standard.

Note that the geometries created by the manipulator against the real measurement pattern show that the highest standard error was obtained for parallel lines spaced 10 mm (6.4%). Thereafter, there was a significant decrease in the error for the 15-mm distance (1.8%). Increasing the distance led to similar errors, reaching 1.8%,



1.5%, 1.6%, and 0.9%, respectively. The error for the largest gap was twice that of the previous three. Regarding the mapping of the right angle, an error of 0.2% can be observed. As in the case of measurements of the standard itself, it can be stated that the implementation of the geometric real dimensions became more accurate with the increase in the distance between the created geometries. The relative error did not exceed 7.0% in any case, reaching a maximum of 6.4% for the smallest geometry, and decreasing by a factor of 5 for the largest distances.

A plot was constructed to illustrate the distribution of the standard deviation (Fig. 13).

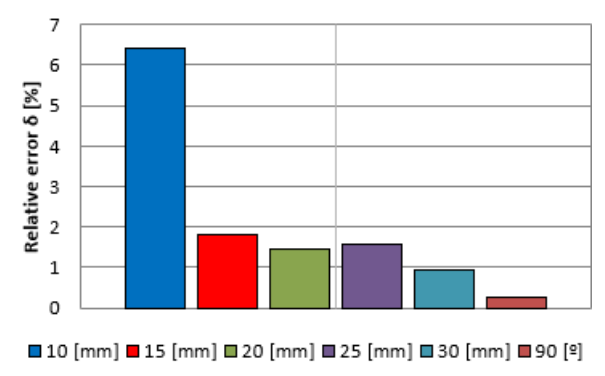


Fig. 12. Relative error robot - reference

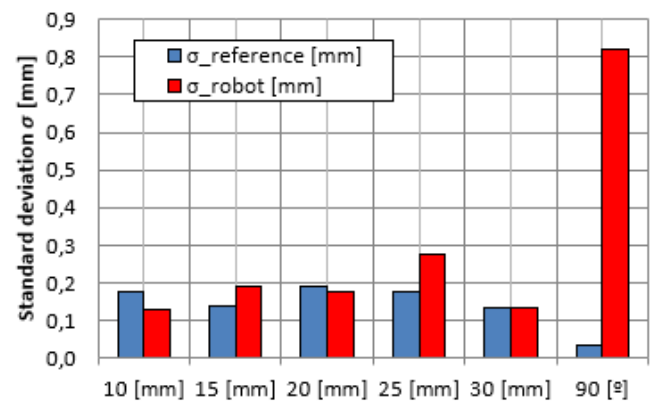


Fig. 13. Standard deviation distribution

Standard deviation is the usual criterion to determine the variability of results. It provides information about spreading and its distribution for the results obtained around the mean of measurements. In accordance with the distributions shown in Fig. 13, it can be concluded that the standard deviations for real standard measurements as well as for geometry measurements made by the robot related to the parallel lines are similar. The standard deviation did not exceed 0.2 except for lines 25 mm apart. However, this increase was small (0.274) and did not affect the overall analysis. A larger standard deviation can be observed for the measurements at 90° (0.819°). Despite the smallest relative error, the volatility of the results around the average is notably high (it remains low compared to the global results).

Additionally, Fig. 14 shows the mean values of each geometry with the corresponding error range and resolution – the maximum and minimum values for both the measurement pattern and geometry made by the manipulator.

Thus, it is possible to determine the range in which the obtained values fell. As emphasized in the previous analysis, the values of the pattern and geometry intervals made by the manipulator are

similar, which proves that the measurements were properly made, and the positioning accuracy was high. With respect to the dispersion of the reference values, a greater dispersion was registered for the value at 90° – a difference of 3,2° that, given the size of the angle, it is insignificant and acceptable.

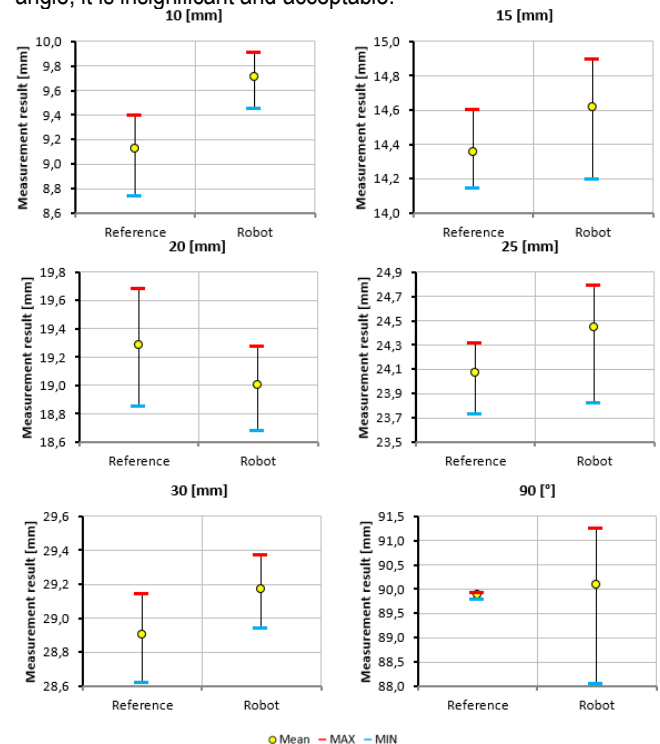


Fig. 14. Variability of measurement results for the analyzed geometries

4.2. Results of second construction

The displacement results obtained from the robot are listed in Table 3. These results include all the displacements performed in individual distance cycles and calculations made on the basis of obtained values. In addition, statistical parameters were again considered, such as standard deviation, skewness, and kurtosis. The experimental results are presented in Fig. 15. Before starting the execution of the individual cycle in automatic mode, the distance of the element transferred during the learning procedure was measured. Table 3 considers the above carrying lengths: 84.0, 121.2, and 204.2 mm.

Tab. 3. Calculations of measurement results of element displacement by the robot

	Distance 1	Distance 2	Distance 3
	84.0 mm	121.2 mm	204.2 mm
Mean	83.883	121.393	204.587
Max	84.518	121.446	204.763
Min	83.490	121.352	204.400
R	1.027	0.094	0.363
σ	0.378	0.027	0.117
Α	0.642	0.861	-0.165
K	-1.060	-0.526	-1.270
$U_{0.95}$	0.135	0.010	0.042

\$ sciendo

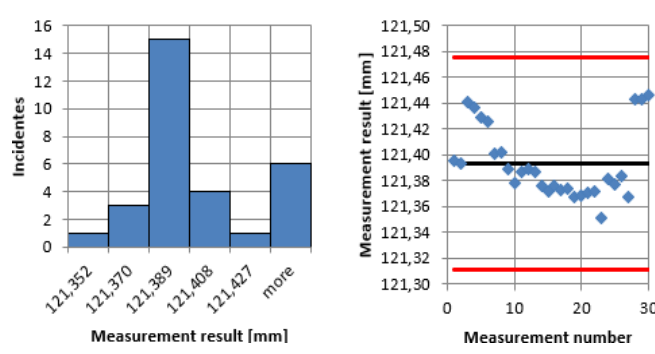


Fig. 15. Value distribution histogram (left side) and distribution of the result values $\pm 3\sigma$ (right side) for a displacement of 121.2 mm

According to Table 3, the average values for the second and third items were above the set value, whereas for the first item, they were below the set value. The deviations from the set value were $84.0^{+0.518}_{-0.510}$; $121.2^{+0.246}_{+0.152}$; $204.2^{+0.563}_{+0.200}$. The lowest values for both the maximum and minimum deviations were recorded at 121.2 mm. The positioning tolerance for the obtained results was also smallest for the middle distance (0.094 mm). The worst result was recorded for the smallest distance, 84.0 mm; it was 1.027 mm. For extreme maximum distance, that is, 204.2 mm, a tolerance of 0.117 mm was obtained. The difference between the mean and set values was the smallest for the minimum considered distance; this difference was 0.117 mm. These are similar results to the first case, but with a positive value for 121.2 mm: 0.193 mm. The worst distance in this comparison was the maximum one, for which the result was 0.387 mm.

The smallest skewness, as a parameter defining the nature of the dispersion of data distribution from the resulting samples, was recorded successively for 204.2 mm, 84.0 mm, and 121.2 mm. For the third distance, the skewness is left-handed, indicating a slight dispersion of the results above the average. For the first and second items, right-handed dispersion of results below the average was obtained. The histogram (Fig. 15) for the second item takes an asymmetric form, close to the normal distribution, with a clear peak reached for the values in the range 121,389 mm. Accordingly, it can be concluded that the mean value (121.393 mm) was recorded on one side of the distribution. This proves that the lower limit of the results and the density of the measurements close to the average values were maintained. Additionally, it can be observed in Fig. 15 that most of the measurement points revolve around the mean value. Importantly, for all items and trials, no single result exceeding ±3σ was observed. This was confirmed by the distribution of the values. It can be clearly observed that most of the measurements were at or below the mean value.

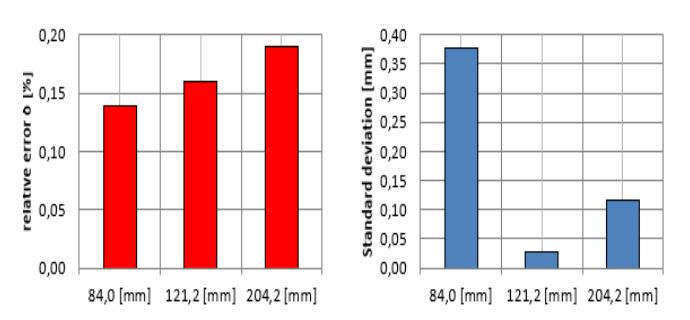


Fig. 16. Distribution of the relative error (left side) and standard deviation (right side)

As shown in Fig. 16, the lowest variability of the observed results was recorded successively for displacements of 121.2 mm, 204.2 mm, and 84.0 mm. The standard deviations were 0.027 mm, 0.117 mm, and 0.378 mm, respectively. An important fact is the increasing nature of the relative error (Fig. 16). For distance 1 (84.0 mm), distance 2 (121.2 mm), and distance 3 (204,2 mm), the errors were 0.14%, 0.16%, and 0.19%, respectively.

5. CONCLUSIONS

This paper presents possibilities of applying a proprietary control algorithm to two different de-signs of RRR manipulators. Correlations were found between the implementation of the distance between the start and end points of individual trajectories and the actual implementation of the manipu-lator's movements.

Analysis of the first proposed structure shows that the worst standard deviation results were ob-tained for a distance in the middle of the interval. However, a relative error was observed for the shortest distance. Owing to the design changes introduced, it was possible to reduce the standard devi-ation in the middle range of the working area at the expense of that in the upper range. Comparing the second structure with the first one, the relative error in the lower range of the working area was signif-icantly reduced, reaching its lowest value for all the displacements.

For both structures, a negative kurtosis was maintained for all the displacements. Thus, it was pos-sible to determine both the distribution and concentration of the results. Negative kurtosis values indi-cate a platykurtic distribution and a lack of outliers, which strongly proves the clustering of results around the mean value.

An important parameter in a distribution is skewness. A skewness coefficient below 0 indicates left-handed asymmetry of the distribution. This means that most of the results are above the average. In case of coefficient values above 0 (right-handed distribution), most results are below the mean. For both structures, negative values of skewness were obtained for all trajectories (except for the positions of the first and second structures, which remained close to 0). The difference in the results for the 84.0-mm and 121.2-mm trajectories was due to a structural change and deliberate change in the standard deviation and relative error by a design change at the expense of other parameters. For both designs, the individual positioning tests were inside the mean $\pm 3\sigma$ interval. According to this analysis, a high level of repeatability and concentration of results was confirmed.

The algorithm for the first construction enabled the learning process to be maintained and repro-duced in automatic mode below ± 1.0 mm, taking into account the measurement of the pattern itself as well as the measurement of the implementation of the marker trajectory. However, for the second structure, the results were below ± 0.6 mm.

The research conducted using all the applications, advanced multisensory equipment, measure-ment methods, and statistical analysis, has proven that the application of the same algorithm to two different designs does not have to negatively affect the resulting positioning quality. By respecting the calculation rules of both the trajectory of movements and geometric dimensions of the manipulator as well as the working area, with the same program executing the manipulator's movement, it is possible to improve positioning parameters by interfering only with the mechanical structure. The statistical calculations used during the analysis of the results confirmed the assumptions related to the analysis of

DOI 10.2478/ama-2025-0045

positioning quality and repeatability of the manipulator movement trajectory in automatic mode.

In the subsequent stages of research, particular emphasis will be placed on two key issues that may significantly influence the further optimization of accuracy and reliability in the operation of robotic manipulators in advanced industrial environments.

First, the application of a photogrammetric system is planned for the precise determination of the spatial positions of individual nodes within the manipulator's kinematic structure. This approach will enable high-resolution reconstruction of the robot's geometry and accurate mapping of its actual motion trajectory, thereby allowing for a detailed analysis of deviations from the pre-programmed paths. Photogrammetry, as a non-contact and high-precision measurement method, will be essential for evaluating spatial relationships and identifying potential kinematic discontinuities under real operating conditions.

Second, the impact of the payload mass on positioning accuracy will be examined. This factor is of crucial importance in real-world industrial applications, where variations in the carried load can cause structural deflections and inertial effects, which in turn negatively affect trajectory tracking accuracy. The planned studies will include manipulation tests under various payload conditions to assess the extent to which load mass affects the stability and precision of positioning. These analyses will be conducted using two independent measurement systems: a multisensor coordinate measuring machine (CMM) and a photogrammetric system. This dual-approach will allow for cross-verification of results and provide a comprehensive evaluation of the applicability and accuracy of both methods in the context of dynamic and spatial measurements.

The findings obtained from this research will make a significant contribution to the development of universal and adaptive control algorithms capable of compensating for structural deformations and trajectory disturbances caused by variable load conditions. The ultimate goal of these activities is to enhance the precision, flexibility, and reliability of robotic systems used within the framework of Industry 4.0.

REFERENCES

- Fromhold-Eisebith M, Marschall P, Peters R, Thomes P. Torn between digitized future and context dependent past – How implementing 'Industry 4.0' production technologies could transform the German textile industry. Technological Forecasting and Social Change. 2021;166:120620. https://doi.org/10.1016/j.techfore.2021.120620
- Müller JM, Buliga O, Voigt K-I. Fortune favors the prepared: How SMEs approach business model innovations in Industry 4.0. Technological Forecasting and Social Change. 2018;132:2–17. https://doi.org/10.1016/j.techfore.2017.12.019
- Engemann H, Du S, Kallweit S, Cönen P, Dawar H. OMNIVIL—An Autonomous Mobile Manipulator for Flexible Production. Sensors. 2020;20(24):7249. https://doi.org/10.3390/s20247249
- Hanh LD, Tu HB. Computer Vision for Industrial Robot in Planar Bin Picking Application. Advances in Science, Technology and Engineering Systems Journal. 2020;5(6):1244–9. https://doi.org/10.25046/aj0506148
- Bedaka AK, Mahmoud AM, Lee S-C, Lin C-Y. Autonomous Robot-Guided Inspection System Based on Offline Programming and RGB-D Model. Sensors. 2018;18(11):4008. https://doi.org/10.3390/s18114008
- Engemann H, Wiesen P, Kallweit S, Deshpande H, Schleupen J. Autonomous Mobile Manipulation Using ROS. In: Advances in Service and Industrial Robotics. Cham: Springer International Publishing; 2017. p. 389–401. [accessed 4 Apr 2024] https://doi.org/10.1007/978-3-319-61276-8 43

- Bedaka AK, Vidal J, Lin C-Y. Automatic robot path integration using three-dimensional vision and offline programming. The International Journal of Advanced Manufacturing Technology. 2019;102(5– 8):1935–50. https://doi.org/10.1007/s00170-018-03282-w
- Jermak CzJ, Jakubowicz M, Dereżyński J, Rucki M. Air Gauge Characteristics Linearity Improvement. Journal of Control Science and Engineering. 2016;2016:1–7. https://doi.org/10.1155/2016/8701238
- Jakubowicz M, Rucki M, Varga G, Majchrowski R. Influence of the Inlet Nozzle Diameter on the Air Gauge Dynamics. In: Lecture Notes in Mechanical Engineering. Cham: Springer International Publishing. 2017; 733–42. [accessed 2024] https://doi.org/10.1007/978-3-319-68619-6 71
- Arnarson H, Solvang B. Reconfigurable autonomous industrial mobile manipulator system. In: 2022 IEEE/SICE International Symposium on System Integration (SII). IEEE; 2022. [accessed 4 Apr 2024] https://doi.org/10.1109/sii52469.2022.9708887
- Teixeira FM, Silva MF. Simulation of a Robotic Co-transport System.
 In: 2021 IEEE International Conference on Autonomous Robot Systems and Competitions (ICARSC). IEEE; 2021. [accessed 4 Apr 2024] https://doi.org/10.1109/icarsc52212.2021.9429776
- Häuschen H. Der Bauksten . Industieroboter im praktischen Einsatz. Proc 3rd ISIR. 1973;83–93.
- 13. Warnecke H, Schraft R. Einlegegeräte zur automatischen. Mainz : Krausskopf-verlag; 1973.
- Feix T, Romero J, Schmiedmayer H-B, Dollar AM, Kragic D. The GRASP Taxonomy of Human Grasp Types. IEEE Transactions on Human-Machine Systems. 2016 Feb;46(1):66–77. https://doi.org/10.1109/thms.2015.2470657
- Hua J, Zeng L, Li G, Ju Z. Learning for a Robot: Deep Reinforcement Learning, Imitation Learning, Transfer Learning. Sensors. 2021;21(4):1278. https://doi.org/10.3390/s21041278
- Rękas A, Kaczmarek T, Wieczorowski M, Gapiński B, Jakubowicz M, Grochalski K, et al. Analysis of Tool Geometry for the Stamping Process of Large-Size Car Body Components Using a 3D Optical Measurement System. Materials. 2021;14(24):7608. https://doi.org/10.3390/ma14247608
- Swojak N, Wieczorowski M, Jakubowicz M. Assessment of selected metrological properties of laser triangulation sensors. Measurement. 2021;176:109190. https://doi.org/10.1016/i.measurement.2021.109190
- Grochalski K, Wieczorowski M, Jakubek B. Influence of thermal disturbances on profilometric measurements of surface asperities. Measurement. 2022 Feb;190:110694. https://doi.org/10.1016/j.measurement.2021.110694
- Jakubek B, Barczewski R, Jakubowicz M. The influence of the lubrication on the vibroacoustic signal generated by rolling bearings. Vibrations in Physical Systems . 2017;28:1–9.
- Andrzejewski J, Marciniak-Podsadna L. Development of Thermal Resistant FDM Printed Blends. The Preparation of GPET/PC Blends and Evaluation of Material Performance. Materials. 2020;13(9):2057. https://doi.org/10.3390/ma13092057
- Chen X, Huang Z, Sun Y, Zhong Y, Gu R, Bai L. Online on-Road Motion Planning Based on Hybrid Potential Field Model for Car-Like Robot. Journal of Intelligent & Systems. 2022;105(1). https://doi.org/10.1007/s10846-022-01620-5
- Maini P, Gonultas BM, Isler V. Online Coverage Planning for an Autonomous Weed Mowing Robot With Curvature Constraints. IEEE Robotics and Automation Letters. 2022 Apr;7(2):5445–52. https://doi.org/10.1109/lra.2022.3154006
- Mitsi S, Bouzakis K-D, Mansour G, Sagris D, Maliaris G. Off-line programming of an industrial robot for manufacturing. The International Journal of Advanced Manufacturing Technology. 2004;26(3):262–7. https://doi.org/10.1007/s00170-003-1728-5
- Larkin N, Milojevic A, Pan Z, Polden J, Norrish J. Offline programming for short batch robotic welding. In: 16th joining of materials (JOM) conference. 2011.
- Wang C, Zhang Y, Zhang X, Wu Z, Zhu X, Jin S, et al. Offline-Online Learning of Deformation Model for Cable Manipulation With Graph Neural Networks. IEEE Robotics and Automation Letters.



Improvement and Control Trajectory Tracking of a Three-Axis Manipulator for New Training Strategies

- 2022;7(2):5544-51. https://doi.org/10.1109/lra.2022.3158376
- Wang Z, Tian G. Hybrid offline and online task planning for service robot using object-level semantic map and probabilistic inference. Information Sciences. 2022;593:78–98. https://doi.org/10.1016/j.ins.2022.01.058
- Javaid M, Haleem A, Singh RP, Suman R, Gonzalez ES. Understanding the adoption of Industry 4.0 technologies in improving environmental sustainability. Sustainable Operations and Computers. 2022;3:203–17.
 - https://doi.org/10.1016/j.susoc.2022.01.008
- Tipary B, Erdős G. Tolerance analysis for robotic pick-and-place operations. The International Journal of Advanced Manufacturing Technology. 2021;117(5–6):1405–26. https://doi.org/10.1007/s00170-021-07672-5
- Mohsen M, Mohamed AM, Ahmed SM, Ibrahim K. Bilateral Control Of A 2-Dof Teleoperated Manipulator Using Udp Scheme. Ain Shams Engineering Journal. 2023;14(9):102065. https://doi.org/10.1016/j.asej.2022.102065
- Sun Y, Wan Y, Ma H, Liang X. Workspace Description and Evaluation of Master-Slave Dual Hydraulic Manipulators. Actuators. 2022;12(1):9. https://doi.org/10.3390/act12010009
- Li Z, Zhang E, Zhai B, Li B. Master-Slave Arm Heterogeneous Mapping With Link Pose Constraint in Teleoperation System. IEEE Access. 2022;10:107202–13. https://doi.org/10.1109/access.2022.3213054
- Wang J, Li H, Meng F, Ma R, Lai Q, Li J, et al. Control Strategy of Master-Slave Manipulator Based on Force Feedback for Decommissioning of Nuclear Facilities. Mathematical Problems in Engineering. 2022;2022:1–9. https://doi.org/10.1155/2022/9945758
- Jin X, Guo S, Guo J, Shi P, Kawanishi M, Hirata H. Active Suppression Method of Dangerous Behaviors for Robot-Assisted Vascular Interventional Surgery. IEEE Transactions on Instrumentation and Measurement. 2022;71:1–9. https://doi.org/10.1109/tim.2022.3170997
- Shi H, Zhang B, Mei X, Song Q. Realization of Force Detection and Feedback Control for Slave Manipulator of Master/Slave Surgical Robot. Sensors. 2021;21(22):7489. https://doi.org/10.3390/s21227489
- Azizi A, Latifinavid M. Hybrid Artificial Intelligence Algorithm for Optimizing RFID Network Planning in Smart Manufacturing. Journal of Robotics. 2020;2020:1–14. https://doi.org/10.1155/2020/8564140
- Azizi A, Latifinavid M. Artificial Neural Network Approach for Dynamic Behavior Optimization of Robotic Arms in Industry 4.0. Journal of Robotics. 2017;2017:1–10. https://doi.org/10.1155/2017/8728209
- Latifinavid M, Azizi A. Development of a Vision-Based Unmanned Ground Vehicle for Mapping and Tennis Ball Collection: A Fuzzy Logic Approach. Future Internet. 2023;15(2):84. https://doi.org/10.3390/fi15020084
- Azizi A, Latifinavid M. Ring Probabilistic Logic Neural Network for Active Suspension Control in Vehicles. In: Ahram T, Taiar R, Colson S, Choplin A eds. Advances in Intelligent Systems and Computing. Singapore: Springer. 2019;943:35–45. https://doi.org/10.1007/978-981-13-2640-0_4
- Kim Y-S, Dagalakis NG, Marvel J, Cheok G. Design and Testing of Wireless Motion Gauges for Two Collaborative Robot Arms. Measurement Science Review. 2022;22(2):84–91. https://doi.org/10.2478/msr-2022-0011
- Liu Q, Guo H, Ma Y, Tian W, Zhang Z, Li B. Real-time error compensation of a 5-axis machining robot using externally mounted encoder systems. The International Journal of Advanced Manufacturing Technology. 2022;120(3–4):2793–802. https://doi.org/10.1007/s00170-022-08867-0
- Wang X, Li H, Zhang Y. 3D Scanning Based Precision Evaluation of Industrial Robots. Robotics and Computer-Integrated Manufacturing. 2019; 56; 123–130. https://doi.org/10.1016/j.rcim.2018.10.007

- Chen J, Zhou F, Wu X. Multisensor Measurement System for Robot Positioning Accuracy Assessment. Sensors. 2020;20(4);1015. https://doi.org/10.3390/s20041015
- Li M, Xu W, Chen L. (2018). Integration of Structured Light scanning in Robot Trajectory Control for Enhanced Precision. IEEE Transactions on Industrial Electronics. 20188; 65(8): 6712–6720. https://doi.org/10.1109/TIE.2017.2787563
- Chang Q, Gao X, Liu Y, Deng J, Zhang S, Chen W. Development of a cross-scale 6-DOF piezoelectric stage and its application in assisted puncture. Mechanical Systems and Signal Processing. 2022;174:109072. https://doi.org/10.1016/j.ymssp.2022.109072
- 45. LI H, Xu Y, Zhang C, Yang H. Kinematic modeling and control of a novel pneumatic soft robotic arm. Chinese Journal of Aeronautics. 2022;35(7):310–9. https://doi.org/10.1016/j.cja.2021.07.015
- Jakubowicz M. Accuracy of roundness assessment using air gauge with the slot-shaped measuring nozzle. Measurement. 2020 Apr;155:107558. https://doi.org/10.1016/j.measurement.2020.107558
- Dietrich E, Schulze A. Statistical Procedures for Machine and Process Qualification. 1st ed. Munich: Hanser Publications; 2010.

This study, conducted under subject No. 0614/SBAD/1586, was funded by grants for education allocated by the Ministry of Education and Science in Poland.

Patryk Mietliński: https://orcid.org/0000-0002-2300-0834

Michał Jakubowicz: https://orcid.org/0000-0002-6350-0411

Lidia Marciniak-Podsadna: https://orcid.org/0000-0002-4444-0724

Michał Wieczorowski: https://orcid.org/0000-0001-7526-8368



This work is licensed under the Creative Commons BY-NC-ND 4.0 license.